Application Note 41

Multimodal Ultrafast Spectroscopy System Based on a 35 Femtosecond Ti:Sapphire Chirped Pulse Amplification (CPA) Laser

Technology and Applications Center
Newport Corporation

Spectra-Physics
A Division of Newport Corporation

Newport
Experience | Solutions

Introduction

With technology pushing laser pulse durations into the femtosecond regime[1], the development of methods for time-resolved ultrafast nonlinear spectroscopy to determine the dynamics of atomic and molecular systems seems inevitable. While X-ray crystallography[2] and NMR spectroscopy[3,4] have provided unprecedented information on the structures of molecules and revealed dynamics in micro-to-millisecond time scales, ultrafast nonlinear spectroscopy serves as a complementary tool for understanding the molecular dynamics on femto- to nanosecond time scales. Ingenious methodologies utilizing the principles of ultrafast spectroscopy[5] have boosted our understanding in physical science. Fruitful applications span a wide spectrum including photophysics, photochemistry, high-energy physics, femtobiology, and medical science, just to name a few[6,7]. With the way well paved, the development of new methodologies is ongoing, promising and presents exciting challenges for researchers.

Within the last decade, amplified femtosecond lasers based on chirped pulse amplification (CPA)[8] have advanced the average power and energy per pulse to several Watts and mJ respectively, while the pulses have become shorter. Lasers with 25 fs pulse width and 5-7 mJ energy at 1 kHz repetition rate are commercially available. However, amplified femtosecond lasers remain complex and expensive. Due to this reason, the trend in ultrafast spectroscopy labs is to use such a laser for multiple experiments by dividing the laser beam and setting up independent experiments. Multi-user setups allowing shared cost of ownership will become more common. Accordingly, flexible ultrafast spectroscopy setups enabling multimodality have never been more important.

In this application note, we describe an ultrafast multimodal spectroscopy system based on an amplified 35 fs Ti:Sapphire laser allowing multiple independent, concurrent experiments. We demonstrate the performance and feasibility of the system by presenting experimental studies of colloidal gold nanoparticles, neat liquids and solutions, while employing transient absorption, spatially masked Kerr lens (SMKL), femtosecond stimulated Raman scattering (SRS), and coherent anti-Stokes Raman scattering (CARS) methods.

II. Method and Experimental Setup:

The multimodal spectroscopy system is based on a Ti:Sapphire chirped pulse amplifier (Spectra-Physics Spitfire® Pro 35) operating at 1 kHz repetition rate and generating 35 fs pulses centered around 800 nm. The diagram of the setup is shown in Figure 1. The laser produces 3.5 W of average power with 3.5 mJ energy per pulse at 1 kHz repetition rate. The output is divided into four beams of approximately equal intensity providing 850 µJ pulse energy per beam. One of the beams is maintained at 800 nm or can be frequency doubled. Two of the beams are used to pump two optical parametric amplifiers (Spectra-Physics TOPAS™). The fourth beam is coupled into Newport's Helios™ transient absorption spectrometer.

For stable operation of the OPAs and the white light based transient absorption spectrometer, the laser beam size, divergence and pulse energy have to be carefully adjusted. This is accomplished by means of telescopes, beamsplitters and routing mirrors optimized for ultrafast pulses. In order to achieve the best performance out of the system, it is critical to pay attention to the beam handling details.

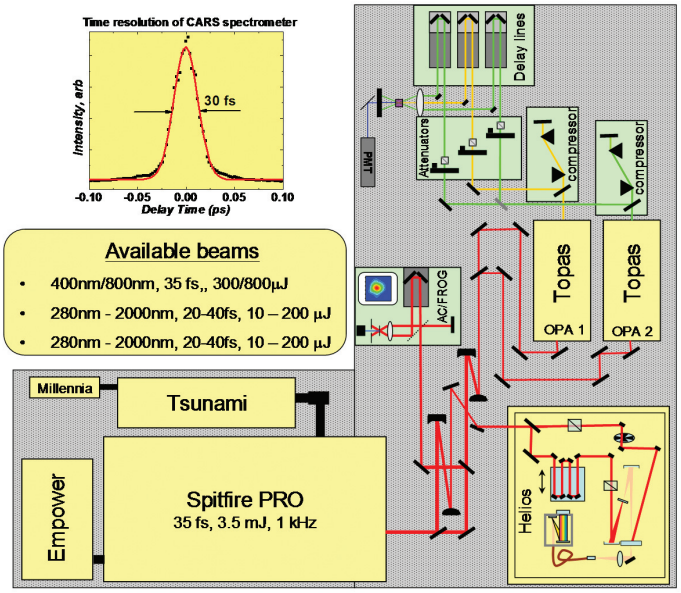

Figure 1. Block diagram of the experimental setup. The laser output is divided into four beams used to pump two OPAs, the Helios transient absorption spectrometer, and additional diagnostic tools. The system consists of modules that can be easily reconfigured.

With a beam diameter of ~10 mm and pulse widths as short as 35 fs, the peak power reaches about 100 GW/cm^2. Dividing the beam into four paths requires the use of beamsplitters, entailing that a significant part of the beam passes through the substrates. Large beam size precludes the use of 1" optics, especially when the incidence angle is at 45 degrees and the clear apertures are reduced. Additionally, to avoid wavefront distortions, beamsplitters with substrate thickness < 5 mm are required. However, after passing through a thick substrate, in addition to temporal distortions introduced by the high-order dispersion of the substrate material, significant distortions of the beam are expected due to self-focusing and self-phase modulation. To optimize performance, we utilized Newport's FROG kit (FRG-KT) to conduct a detailed characterization of the laser pulses before and after propagation through various substrates of different thickness and material.

A small part of the output beam was picked off and sent to the FROG device. A variable neutral density filter was used to further attenuate the beam. The FROG trace of the unperturbed laser pulse picked off at the output of the amplifier is presented in Figure 2a. After inserting an 8 mm thick fused silica (FS) substrate into the beam at the output of the laser and before the pick-off mirror, the FROG trace showed significant elongation of the pulse (Figure 2b). The pulse was then recompressed by adjusting the distance between the gratings in the compressor inside the amplifier (Figure 2c), but still showed significant elongation.

Alternatively, the same measurement was repeated, though in this instance the beam was first attenuated, and subsequently passed through the 8 mm FS substrate prior to the FROG (Figure 2d). In this case, with the beam intensity lowered, the original pulse characteristics can be completely recovered. This is in sharp contrast with the initial case where the high energy pulse was passed through the same substrate. Absence of significant differences between the traces in Figure 2a and Figure 2d means that the distortion of the pulse through the substrate is mainly due to high peak power. We performed similar measurements for 8 mm thick BK7, 3 mm BK7 and 3 mm FS substrates. The results showed that only the 3 mm FS substrate is suitable for the first and second beam splitter after the amplifier.

We also performed Z-scan characterization of the BK7 and FS substrates (refer to application note 34). Under the same conditions, the BK7 substrate exhibited noticeable two-photon absorption. After several hours of exposure to laser pulses, the BK7 showed considerable color center formation followed by optical damage. In our setup, we therefore used only 3 mm thick FS substrates. Similar constraint should be applied in choosing optics for telescopes or focusing. As a result, we used only reflective curved mirrors for these purposes.

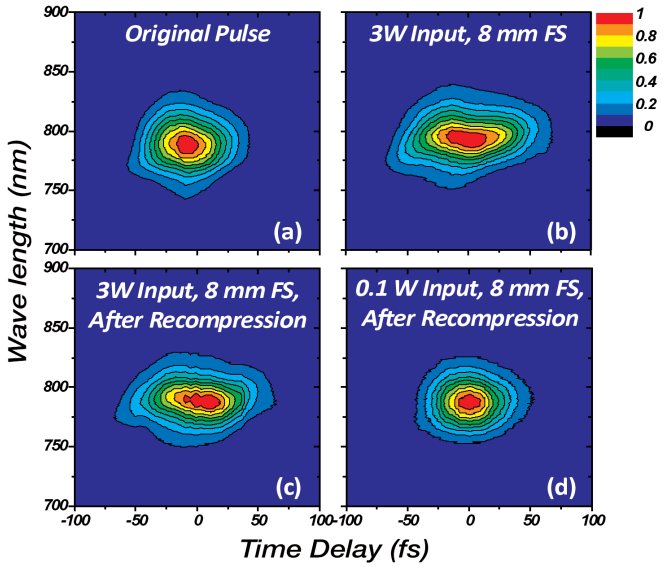

Figure 2. FROG traces of the original 35 fs/3 mJ pulse (a), after initially passing through 8 mm thick fused silica substrate (b), and after recompression by adjusting the grating compressor inside the amplifier (c). FROG trace of the 100x attenuated pulse after passing through the same substrate (d).

II-1. Transient Absorption Spectrometer:

Transient absorption experiments utilize two laser pulses (pump and probe) with adjustable time-delay between them. The pump pulse interacts with the system of interest, after which the time-dependent transient change of the absorption of the system is monitored by the probe beam. This transient change contains clues to both structural information and dynamics. The pulse-to-pulse stability of the laser is of prime importance since the measurement is based on the change of the probe pulse profile (difference of probe pulse profile with and without pump). The time resolution of the system is defined by the pulse duration. The advent of shorter pulses resulted in the capability to interrogate molecular motion with great detail.

Measurements over a broad spectral range are highly desirable, as they allow for more accurate interpretation of data. While this can be achieved by using OPAs to tune both pump and probe to cover the spectral range, the data collection time becomes onerous, especially when long time scans with high resolution are required. On the other hand, using a broadband supercontinuum (white light) as a probe allows detection of the sample absorption in a wide spectral range at one shot. Furthermore, fast data acquisition electronics combined with fast photodiode arrays or CCD chips enables massive data transfer into the computer to take advantage of the increased information gathered in this technique in a far shorter experimental time.

Newport's Helios transient absorption spectrometer is based on fixed-wavelength pump and supercontinuum probe beams. The diagram of the device is shown in Figure 3.

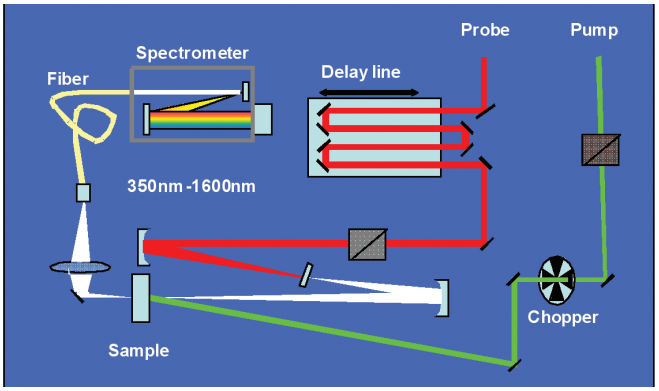

Figure 3. Diagram of the transient absorption spectrometer. A small portion of the beam is used to generate a supercontinuum as the probe beam. The transmitted beam is analyzed with a fiber coupled spectrometer.

One of the four beams out of the amplifier is used as the pump to excite the sample at 800 nm or at the doubled frequency of 400 nm. Alternatively, an OPA can be used to excite the sample in the wavelength range from 240 nm to 800 nm. In either case, the pump beam is routed through a chopper which is synchronized with the laser. A small portion of the 800 nm pump beam is picked off for use as a probe beam. It is sent through a double-pass delay line and then focused into crystalline material to generate supercontinuum. A 2 mm thick sapphire window is used to generate a UV-VIS spectrum or a 20 mm CaF_2 crystal is used to generate a NIR spectrum. The generated supercontinuum is then focused into the sample and overlapped with the pump beam. After that it is coupled into a diode array based spectrometer. The device can operate in two spectral regimes covering probe wavelengths from 400 nm to 800 nm or 800 nm to 1600 nm. Due to dispersion and self-phase modulation in the substrate, the generated supercontinuum is chirped and stretched to ~ 200 fs.

The optical delay line allows 3.2 ns of total delay with 6 fs resolution. Two consecutive transmitted spectra with pump on and pump off are collected and the wavelength-dependent absorbance difference is calculated and saved for each delay. With two second averaging, a sensitivity of better than 0.1 mOD is achieved.

II-2. Spatially Masked Kerr Lens (SMKL) Spectrometer:

The experimental setup for SMKL spectroscopy is similar to the transient absorption experiment although the processes studied at the molecular level are different. In the transient absorption experiment, where resonant interactions dominate, the pump pulse prepares the excited states and bleaches the ground state of the molecules. In KL spectroscopy, the pump pulse excites vibrational and collective motion of the molecules through an impulsive Raman process. The probe pulse stimulates the radiation of a coherent optical field from the sample in a phase-matched direction $\vec{k}_{sig} = +\vec{k}_{pu} - \vec{k}_{pu} + \vec{k}_{pr}$, which is along the direction of the probe pulse. Due to the co-linearity of the stimulated radiation (signal) and the probe pulse, it serves as a local oscillator (LO) and interferes with the signal; the signal is being heterodyned.

Heterodyned detection has a great advantage; signal amplification. Assuming we are looking at the intensity of the frequency component, Ω, the detector measures:

$$S(\Omega)=\{E_{probe}(\Omega)+E_{signal}(\Omega)\}^2=E^2_{probe}(\Omega)+E^2_{signal}(\Omega)+2E_{probe}(\Omega)E_{signal}(\Omega) \quad (1)$$

In equation (1), $E_{probe}(\Omega)$ is the probe field component at Ω frequency, while $E_{signal}(\Omega)$ is the signal field component at Ω frequency. Since we are measuring the difference of the probe with and without pump, the first term on the right of (1) is subtracted. The second term on the right is negligible since in most cases $E_{probe}(\Omega) >> E_{signal}(\Omega)$. We are left with $2E_{probe}(\Omega)E_{signal}(\Omega)$ which shows that the probe field amplifies the signal field.

KL spectroscopy can also be explained phenomenologically as a nonlinear lens effect. In the presence of an intense pump pulse, a material's index of refraction can be written as $n = n_0 + n_2 I$, where I is the intensity of the pump. For a Gaussian beam, this results in a radially varying index of refraction, which in turn acts to focus or defocus the probe. This effect on the probe can be detected by the tightness of the focus using a dual-diode detector (position-sensitive KL spectroscopy[9]), or the amount of probe transmitted through an aperture in the far field (SMKL spectroscopy[10]). In SMKL, two parameters can be used to optimize the sensitivity of detection: the aperture size and its axial distance from the sample. Since the interaction is nonlinear, the signal emitted from a volume that is smaller than the beam waist of the probe has different radius of phase front curvature and spatial phase dependence compared to the probe beam. By changing the aperture size and the axial distance between the sample and the aperture, the phase difference between the signal and the probe field can be changed. As a result, the transient change is optimized by optimizing the phase contrast.

SMKL spectroscopy, as a derivative of KL spectroscopy, was first demonstrated by Simon and co-workers[9]. It has been proven to be a powerful technique for obtaining the isotropic and anisotropic components of intermolecular Raman spectra in liquids[10]. Recently the SMKL method was also applied in studies of thin films[11]. We have utilized the transient absorption spectrometer (Newport's Helios) as a SMKL spectrometer and used the frequency resolved detection to further advance the technique. The 100 µm diameter fiber serves as an aperture. Adjusting the axial position of the fiber end relative to the coupling lens allows for optimizing the heterodyned signal.

II-3. Femtosecond Stimulated Raman Scattering (SRS) Spectrometer:

Raman spectroscopy[12] is a powerful technique to study the structure and dynamics of photophysical and photochemical processes. However, the small cross-section of the Raman process leads to long acquisition times. Frequently, in the case of an electronically resonant Raman process, the background fluorescence masks the weak Raman signal. These two processes are difficult to separate due to the fact that they are both spontaneous, have no directionality, and overlap in frequency. On the other hand, stimulated Raman scattering (SRS) circumvents the problems of non-directionality and spontaneity. It also enhances the signal by heterodyne detection.

SRS is a third-order nonlinear process requiring two laser pulses in a pump-probe configuration. The process is resonantly enhanced when the difference between the frequencies of the two lasers (pump and probe) equals a molecular vibrational frequency. Pump and probe pulses acting simultaneously prepare a vibrational coherence in the sample, another interaction with the pump stimulates the signal radiation and it propagates in the same direction as the probe pulse. With the advent of femtosecond lasers, a new type of SRS spectroscopy, broadband SRS, became available. In broadband SRS, a spectrally narrowed picosecond laser pulse is used as a pump beam and a broadband femtosecond pulse (tens of femtoseconds) serves as a probe. The broadband approach allows the acquisition of the entire Raman spectrum within a single pulse with spectral resolution defined by the bandwidth of the pump pulse[13-15].

For our experiments we used the Helios transient absorption spectrometer. The IR version of the Helios utilizes supercontinuum generated in CaF_2 as a probe (refer to II-1). It extends from 800 nm to 1600 nm. We inserted a 3 nm band pass filter into the pump beam path centered at 790 nm to achieve 25 cm^{-1} spectral resolution. The rest of the setup is identical to the transient absorption spectrometer. The data acquisition of the spectrometer is based on the differential principle described in section II-1. This approach allows for subtraction of the background and provides a better signal to noise ratio.

For time resolved SRS, additional excitation pulses (actinic pulses) are required, similar to the setup described by Mathies and co-workers[13]. By bringing another pulse (either from the OPA or the residual of the pump pulse), the Helios can be easily modified to perform time resolved SRS.

II-4. Four Wave Mixing (FWM) Spectrometer:

Two main beams out of the amplifier with pulse energies about 850 µJ are used to pump two independently tunable OPAs (Figure 4). The pulse width after each OPA is controlled by a prism compressor to ensure the shortest pulse at the sample. The output of OPA2 is split into two to be used as a pump and probe in the coherent anti-Stokes Raman scattering (CARS) spectroscopy setup or to generate a transient grating in the sample in time-resolved transient grating experiments. The output of OPA1 is also compressed and used as the Stokes beam in CARS experiments, or as a probe beam in transient grating experiments.

By time ordering the three pulses accordingly, different FWM experiments can be performed. The two OPAs were set at ~535 nm and ~560 nm. The 535 nm beam was divided in two, and all three beams were focused into the sample using a 150 mm focal length achromatic lens in BOXCAR geometry. The diaphragm behind the sample blocks the input beams. The coherent beam generated in the sample was focused on the 0.25 µm entrance slit of the monochromator. The signal is recorded using a PMT or CCD camera. The experimental FWM signal generated in a microscope slide when all 3 pulses overlap in time is also shown in Figure 4. To perform CARS experiments, beams 1 and 3 are overlapped in time and beam 2 is scanned to produce a time trace of the anti-Stokes signal. When beams 1 and 2 are set at zero delay, scanning the delay of beam 3 probes the transient grating in the sample. The time resolution of the setup was determined to be 27 fs by measuring non-resonant electronic CARS signals from a 100 µm thick piece of glass.

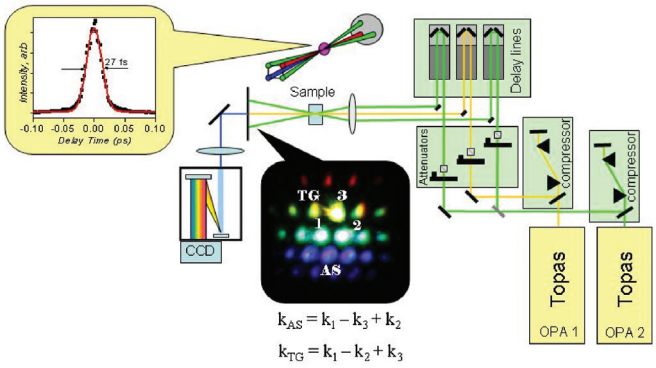

Figure 4. Block diagram of the FWM spectrometer and the signals generated by a microscope slide. Time ordering of the three incident pulses in BOXCAR geometry initiates different types of FWM processes. Overlapping in time beams 1 and 3, and delaying beam 2 results in anti-Stokes beam AS. When beams 1 and 2 are overlapped and beam 3 is delayed, the transient grating signal TG is generated.

Unlike former experiments, the anti-Stokes signal is along a new direction without interfering with the input beams ($\vec{k}_{AS} = +\vec{k}_1 - \vec{k}_3 + \vec{k}_2$). Assuming the signal is composed of Raman modes with frequencies Ω_1 and Ω_2, the detected signal can be described by :

$$S^{sig} = (E_{\Omega_1} + E_{\Omega_2})^2 = E^2_{\Omega_1} + E^2_{\Omega_2} + 2E_{\Omega_1}E_{\Omega_2} \qquad (2)$$

where E_{Ω_1} and E_{Ω_2} are emitted fields associated with Raman modes. The cross term in (2) would produce a delay dependent oscillating signal with frequency Ω_1-Ω_2 and Ω_1+Ω_2. This result is demonstrated in the next section.

III. Results and Discussion:

Gold nanorods in water are used for demonstrating the capabilities of the transient absorption spectroscopy setup, while neat liquid cyclohexane is utilized in the SMKL and SRS experiments. For CARS, we used cyclohexane and carbon tetrachloride to demonstrate the functionality of the experimental setup. Note that the spectral windows covered by SMKL, SRS, and CARS are different. For SMKL, the spectral window is determined by the bandwidth of the pulses. As a result, the dynamics that can be investigated is up to a few hundred wavenumbers. In the case of CARS the spectral window is also determined by the bandwidth of the pulses. However, the center of that window is characterized by the frequency difference of pump and stokes beam. SRS, on the other hand, would cover the entire vibrational window (0 cm^{-1} to more than 3000 cm^{-1}) if stable white light is generated.

III-1. Dynamics of Gold Nanorods in Water:

Plasmon resonances of metallic nanoparticles are the subject of great interest due to the multitude of applications enabled by locally enhanced electric fields and nonlinear optical phenomena mediated by them[16,17]. The optical properties of nanoparticles, summarized by their extinction spectra, depend on size, shape, dielectric medium, and interfacial structure[18]. Aside from the static measurements, the ultrafast response of the nanoparticles after the interaction with electric fields provides valuable information about their properties.

For non-spherical particles, the impulsive heating process induced by the ultrafast pump laser excites multiple vibrational modes. In the case of nanorods, they are the breathing and extensional vibrational modes[19]. The periods of both modes can be expressed as a function of the length and radius of the rods as well as Young's modulus and Poisson's ratio[18]. For well characterized nanorods, their elastic moduli can be completely determined if the periods of both modes are measured. The periods are measured in the following way: the excitation of extensional and breathing modes lead to modulation of electron density and, as a consequence, the transition frequency and bandwidth of the plasmon resonances are modulated[20]. By monitoring the temporal evolution of excited state plasmons through transient absorption spectroscopy, the periods of modulation can be extracted. Thus time-resolved measurements can provide valuable data for extracting the periods of modulation which help us understand the properties of nanoparticles.

We conducted experiments on cylindrical gold nanorods in water. The sample, contained in a 1 mm thick fused silica cuvette, was placed in the overlap region of the pump and probe beams of the transient absorption spectrometer and was constantly stirred. The longitudinal and transverse plasmon bands are spectrally separated, and they can be probed by tuning the probe wavelength or using the supercontinuum probe to cover the entire spectral region. We used 35 fs pulses with center frequency at 795 nm as pump. Transmission of the sample was probed by white light. The results are presented in Figure 5. The two bands on the contour plot correspond to longitudinal (650 nm) and transverse (525 nm) plasmon resonance. A vertical slice (yellow line) along the contour plot shows these resonance frequencies clearly (right graph of figure 5).

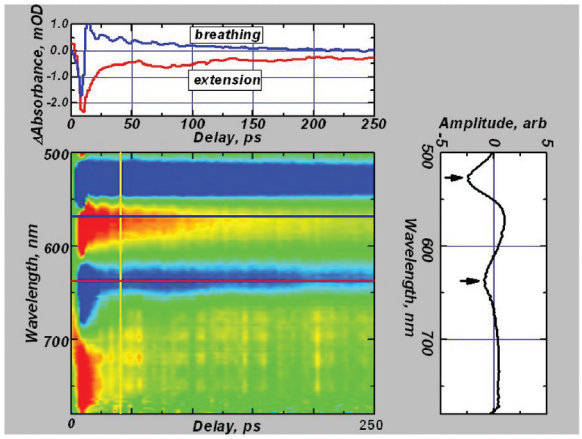

Figure 5. Transient absorption of gold nanorods. Two peaks (right side graph) correspond to longitudinal and transverse surface plasmon resonances at 525nm and 650 nm. Extension and breathing motion of the nanorods can be observed in a single measurement (upper graph).

The two traces in the top graph of figure 5 are horizontal slices of the contour plot along the blue and red lines, respectively. They describe the kinetics of the nanorods' plasmon resonances (transverse and longitudinal plasmon resonance, respectively). These traces exhibit monotonic decay with superimposed oscillations. The blue curve shows distinct oscillations with 13 ps period due to breathing vibration of the nanorods, in agreement with previously published results[18]. The red curve also shows characteristic oscillations with 100 ps period corresponding to the extensional vibration of the nanorods. To the best of our knowledge, this is the first observation of the extension and breathing motion of gold nanorods in one measurement. Further experiments and analysis will be carried out to derive additional information about elastic properties of nanorods.

III-2. SMKL Spectroscopy of Neat Liquids and Solutions:

SMKL spectroscopy was previously applied in studies of the response function of neat liquids, solutions and thin films in non-resonant conditions[10,11]. We further employed the Helios transient absorption spectrometer to demonstrate its additional modality as a SMKL spectrometer. As a sample, we

used cyclohexane. A 1mm thick cuvette with sample was placed inside the Helios transient absorption spectrometer and constantly circulated with a magnetic stirring bar. We used a 35 fs pulse at 800 nm with a bandwidth of 400 cm^{-1} to excite the sample. Time dependent spectra with 2 second average were recorded. The results are shown in Figure 6.

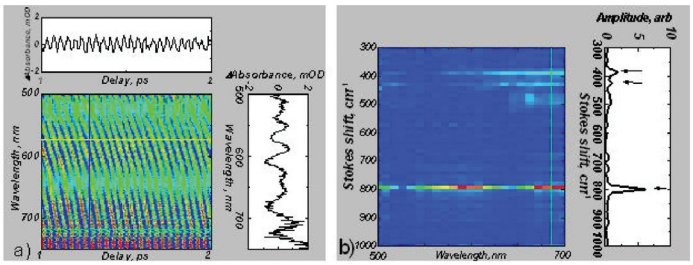

Figure 6. SMKL spectroscopy of cyclohexane. (a) Time dependent oscillations represent signals corresponding to different vibrational modes of the molecule. (b) FFT along the delay shows the fundamental modes which are covered by the bandwidth of the excitation pulse.

The Raman spectrum of cyclohexane has several distinctive peaks. The ones at 384 cm^{-1}, 426 cm^{-1}, 801 cm^{-1} are relevant to this study, since only Raman modes within the spectrum of the excitation pulses are excited. The parallel stripes in Figure 6a represent the oscillating signal due to impulsively excited coherent motion of the molecule. A horizontal slice (yellow line) showed on the top graph presents this distinctive oscillation. The curvature of the stripes is an indication of the chirp in the probing white light, which is stretched to 200 fs. Note, without frequency-resolved detection the time resolution of the setup would be limited to 200 fs and the stripes in the plot would be completely washed out. Ideally, this two-dimensional plot should consist of straight/curved stripes of equal intensity in the case of non-chirped/chirped probe. The complicated pattern on the plot can be explained by irregularities in the phase of the white light. Since white light serves both as a probe and LO field, the irregularities are amplified. A vertical slice (blue line) shows an example of this irregularity.

The FFT of the experimental data along the delay time is also shown in Figure 6b. A vertical slice (cyan line) of the plot shows clearly the fundamental modes of cyclohexane. This supports the argument that the detection is heterodyned. By choosing appropriate polarizations of the pump and probe pulses, this method can also study different tensor elements of the response function of the sample.

To explore the feasibility of the SMKL approach under resonant conditions, we conducted experiments on iodine molecules dissolved in cyclohexane. First, we prepared a concentrated solution of iodine in a small amount of cyclohexane and slowly added the solution to the pure cyclohexane in the cuvette until the transmission of the sample decreased by 50% (1 mm path length). Experimental condition and setup were identical to the nonresonant experiment allowing direct comparison between the two. The results are presented in Figure 7.

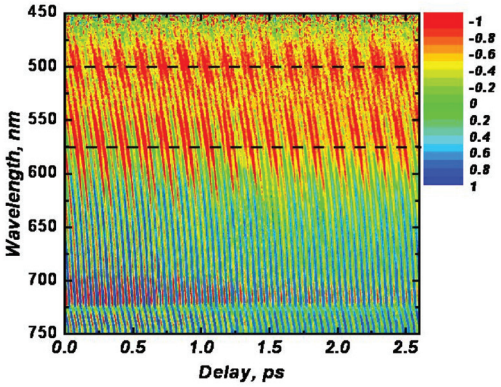

Figure 7. Transient absorption and SMKL spectroscopy of I_2 in cyclohexane. Slow oscillatory motion of Iodine molecule is combined with higher frequency vibrations of cyclohexane molecule at wavelength < 600 nm. The slow oscillation at 500 nm is out of phase compared to that at 575 nm as guided by the dashed lines.

The absorption spectrum of iodine in liquids is structureless due to inhomogeneous line broadening and is centered at ~500 nm. Consequently, at probe wavelengths longer than 600 nm where the probe is off-resonant to the iodine electronic transition, the signal is dominated by oscillatory motion of cyclohexane, analogous to results in Figure 6. With the probe wavelength in the spectral region of iodine electronic transition, signal due to coherent motion of iodine molecules is evident. As can be seen from the upper part of Figure 7, the oscillations caused by iodine vibration enveloped the fast oscillations due to the cyclohexane vibrations. FFT analysis along the horizontal slice (black dashed lines) corroborates the presence of two strong peaks at 801 cm^{-1} (cyclohexane vibration) and 218 cm^{-1} (iodine vibration).

After impulsive excitation, the iodine molecule coherently oscillates until the energy dissipates through phonon coupling with the solvent. Given the bandwidth of the excitation pulse of 400 cm^{-1} and the vibrational frequency of I_2 of 218 cm^{-1}, vibrational states v=1, v=2 and v=3 can be excited. At such low frequency, the coupling with the solvent is weak. Consequently, long lasting coherent oscillations in the ground electronic state can be expected. It is important to point out that the phase of the signals originating from the iodine vibration (the slow oscillation or the envelope of the upper part of figure 7) is wavelength dependent and clearly seen from frequency-resolved SMKL spectroscopy. This can be explained by the wave packet evolution on the ground state potential[21]. For example, the slow oscillatory signals at

probe wavelengths 500 nm and 575 nm are out of phase indicating that the wavepacket in the ground state is observed twice per period of oscillation at the left and right turning points.

III-3. Time Resolved CARS and SRS in Cyclohexane:

In the experiments of neat cyclohexane described above, we used impulsive Raman excitation where only the vibrational modes within the bandwidth of the excitation pulse can be excited. Due to the high sensitivity of the SMKL method, we were able to observe the 801 cm^{-1} mode of the cyclohexane molecule (Figure 6). An alternative approach is to employ femtosecond SRS, as described in II-3. We switched the transient absorption spectrometer to IR mode and used ~0.5 ps pulses centered at 790 nm as a pump and the supercontinuum in the spectral range 800 nm – 1200 nm as a probe. Since the probe beam is strongly chirped, the overlap in time between the pump and probe pulses will occur at different delays. For that reason we recorded the signal dependence on the delay between the pump and probe pulses. The results are shown in Fig. 8. The probe pulse is chirped, and the time overlap of different spectral components of the probe pulse with the pump pulse occurs at different delays. The curved line in Fig. 8a is for illustrative purposes. It shows the approximate wavelength-dependent zero delay position.

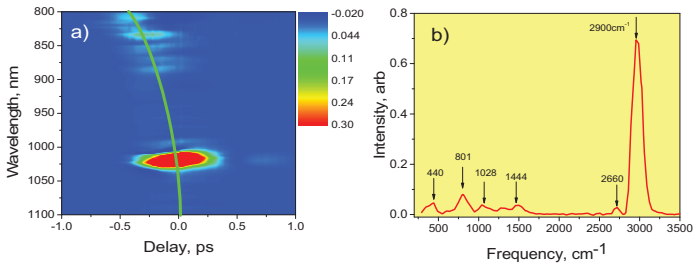

Figure 8. femtosecond SRS of cyclohexane. (a) Contour plot of SRS signal dependence on the delay between the pump and probe pulses. The probe pulse is chirped, and time overlap between different wavelengths of the probe pulse with the pump pulse occurs at different times. The line in (a) is for eye guidance and represents the approximate position of zero delay between the pump and probe pulses. (b) SRS spectrum at zero time delay (the slice along the green line of (a)).

Figure 8b is the spectrum at zero delay between the pump and probe pulses. The arrows indicate positions of known Raman active lines of cyclohexane, as elucidated below. It is evident that there is nearly a perfect match between the peak positions of the spontaneous and stimulated Raman spectra.

In time-resolved CARS, we employed two independently tunable OPAs. The tunability allows the excitation of superposition states centered at Stokes shifts beyond the bandwidth of the pump laser. For example, for the experiments on cyclohexane we tuned the wavelengths of the pump and Stokes beams to 535 nm and 560 nm in order to excite modes centered around 800 cm^{-1} where a few strong vibrational modes of cyclohexane are present. The Raman spectrum of cyclohexane, sketches of vibrational modes, and the covered spectral region are shown in Figure 9. The Raman spectrum is taken with a homemade setup coupled to an Oriel® spectrometer (Oriel Cornerstone™ 260 1/4 m monochromator plus Oriel InstaSpec X CCD).

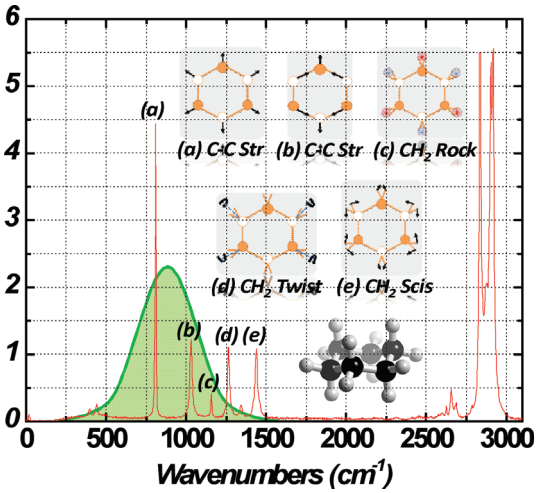

Figure 9. Raman spectrum of cyclohexane. The covered spectral region is shown (shaded green). Also shown are the different vibrational modes contributing to the CARS signal in our measurement.

The recorded CARS signal is presented in Figure 10. The oscillatory signals extended to several picoseconds. The FFT spectra of the signals shown in the insert of Figure 10 exhibit pronounced peaks. According to equation (2), the signals are not heterodyned and we were measuring beating frequencies of the fundamental transitions. For cyclohexane, the characteristic Raman-active peaks covered by our experiments are (a): 801 cm^{-1} (C-C stretch), (b): 1028 cm^{-1} (C-C stretch), (c): 1157 cm^{-1} (CH_2 rock), (d): 1266 cm^{-1} (CH_2 twist), (e): 1444 cm^{-1} (CH_2 scissor). The seven peaks shown in the inset of figure 10 are the beat frequencies between them and are specified on the right side of figure 10. Based on a comparison with spontaneous Raman spectrum, we can conclude that the observed signal is dominated by the beat frequency between these five fundamental modes.

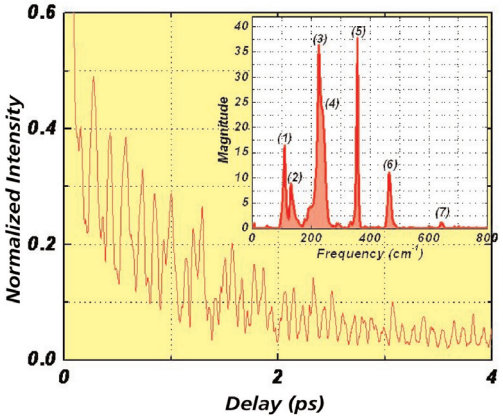

Peak	Beat Frequency
(1)	(d)-(c)
(2)	(c)-(b)
(3)	(b)-(a)
(4)	(d)-(b)
(5)	(c)-(a)
(6)	(d)-(a)
(7)	(e)-(a)

Figure 10. CARS signal from cyclohexane. Raman modes around 800 cm^{-1} are probed. The oscillatory signal is due to a beat between frequencies of C-C stretch (801 cm^{-1}) and other modes of the molecule.

For carbon tetrachloride, we tuned the frequency of one OPA such that the difference in frequencies between the two OPAs covered the fundamental modes of CCl_4 centered at ~ 450 cm^{-1}. These modes are (a): 214 cm^{-1}, (b): 313 cm^{-1}, (c): 460 cm^{-1}, and (d): 780 cm^{-1}, respectively. The beat frequencies between them are specified on the right side and inset of figure 11. These types of experiments demonstrate the stability and excellent time resolution of the laser pulses generated from the Spitfire Pro pumped Topas optical parametric amplifier.

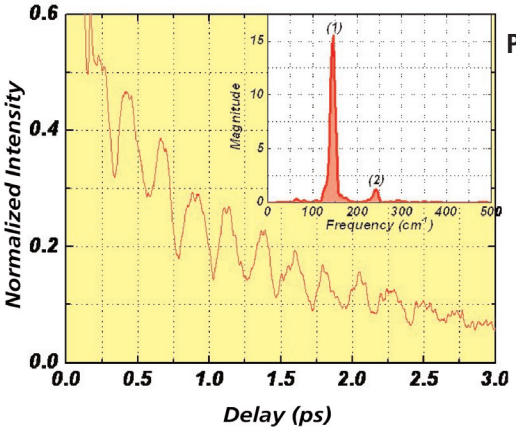

Peak	Beat Frequency
(1)	(d)-(a)
(2)	(c)-(b)

Figure 11. CARS signal from CCl_4. Raman modes ~ 400 cm^{-1} are probed. Again, the oscillatory signal is due to the beat between different vibrational frequencies of CCl_4.

IV. Conclusions:

We have described a multimodal ultrafast spectroscopy system based on an amplified Ti:Sapphire femtosecond laser. The system was proven to produce very stable laser pulses in a wide range of frequencies and can be easily configured for transient absorption experiments and ultrafast nonlinear spectroscopy. Experimental results obtained from studies of neat liquids, solutions and nanoparticles show the robustness and flexibility of such a system. For the first time, we were able to observe breathing and extensional modes of gold nanorods in a single measurement. The resonant enhancement of the signal in frequency-resolved SMKL spectroscopy in liquids was demonstrated. Time traces of the CARS signals also show the superior time resolution of the experiments. The feasibility of employing these methods for third order susceptibility spectroscopy were explored and can be further expanded to multidimensional spectroscopy in the future.

References

1. A. Ducasse, C. Rulliere, and B. Couillaud, *Methods for the Generation of Ultrashort Laser Pulses: Mode-Locking, in Femtosecond Laser Pulses*, (2004), 57-87.
2. B.D. Cullity, *Elements of X-ray Diffraction*. (1978).
3. R.R. Ernst, G. Bodenhausen, and A. Wokaun, *Principles of Nuclear Magnetic Resonance in One and Two Dimensions*. (1987).
4. J.K.M Sanders, and B.K. Hunter, *Modern NMR Spectroscopy*: *A Guide for Chemists.* (1993).
5. S.Mukamel, *Principles of Nonlinear Optical Spectroscopy*. (1995).
6. J.-C. Diels and W. Rudolph, *Ultrashort Laser Pulse Phenomena: Fundamentals, Techniques, and Applications on a Femtosecond Time Scale.* (1996).
7. M.E. Fermann, A. Galvanauskas, and G. Sucha, *Ultrafast Lasers: Technology and Applications*.(2002).
8. G.D. Reid, K. Wynne, Ultrafast Laser Technology and Spectroscopy. *Encyclopedia of Analytical Chemistry*, (2000)13644-13670.
9. Y.J. Chang, P.J. Cong, and J.D. Simon, Isotropic and anisotropic intermolecular dynamics of liquids studied by femtosecond position-sensitive Kerr lens spectroscopy. *Journal of Chemical Physics*, (1997) 106(21): 8639-8649.
10. C.J.Fecko, J.D. Eaves, and A. Tokmakoff, Isotropic and anisotropic Raman scattering from molecular liquids measured by spatially masked optical Kerr effect spectroscopy. *Journal of Chemical Physics* (2002) 117(3): 1139-1154.
11. E. Portuondo-Campa, et al., Ultrafast nonresonant response of TiO_2 nanostructured films. *Journal of Chemical Physics*, (2008) 128(24).
12. D.A. Long, *The Raman Effect: A Unified Treatment of the Theory of Raman Scattering by Molecules.* (2001).
13. D.W.McCamant, P. Kukura, and R.A. Mathies, Femtosecond broadband stimulated Raman: A new approach for high-performance vibrational spectroscopy. *Applied Spectroscopy*, (2003) 57(11): 1317-1323.
14. D.W. McCamant, et al., Femtosecond broadband stimulated Raman spectroscopy: Apparatus and methods. *Review of Scientific Instruments*. (2004) 75(11): 4971-4980.
15. B.Mallick, et al., Design and development of stimulated Raman spectroscopy apparatus using a femtosecond laser system. *Current Science*. (2008) 95(11): 1551-1559.
16. A. Wokaun, J.P. Gordon, and P.F. Liao, Radiation damping in surface-enhanced Raman-scattering. *Physical Review Letters*. (1982) 48(14): 957-960.
17. K. Kneipp, et al., Single molecule detection using surface-enhanced Raman scattering (SERS). Physical *Review Letters*, (1997) 78(9): 1667-1670.
18. S.Link and M.A. El-Sayed, Shape and size dependence of radiative, non-radiative and photothermal properties of gold nanocrystals. *International Reviews in Physical Chemistry*. (2000) 19(3): 409-453.
19. G.V. Hartland, Measurements of the material properties of metal nanoparticles by time-resolved spectroscopy. *Physical Chemistry Chemical Physics*. (2004) 6(23): 5263-5274.
20. R. Zadoyan, et al., Interfacial velocity-dependent plasmon damping in colloidal metallic nanoparticles. *Journal of Physical Chemistry C*. (2007) 111(29): 10836-10840.
21. N.F.Scherer, D.M. Jonas, and G.R. Fleming, Femtosecond wave packet and chemical reaction dynamics of iodine in solution: Tunable probe study of motion along the reaction coordinate. *Journal of Chemical Physics*. (1993) 99(1): 153-168.

Newport Corporation

Worldwide Headquarters
1791 Deere Avenue
Irvine, CA 92606

(In U.S.): 800-222-6440
Tel: 949-863-3144
Fax: 949-253-1680

Email: sales@newport.com

Newport
Experience | Solutions

Visit Newport Online at: **www.newport.com**

This Application Note has been prepared based on development activities and experiments conducted in Newport's Technology and Applications Center and the results associated therewith. Actual results may vary based on laboratory environment and setup conditions, the type and condition of actual components and instruments used and user skills.

Nothing contained in this Application Note shall constitute any representation or warranty by Newport, express or implied, regarding the information contained herein or the products or software described herein. Any and all representations, warranties and obligations of Newport with respect to its products and software shall be as set forth in Newport's terms and conditions of sale in effect at the time of sale or license of such products or software. Newport shall not be liable for any costs, damages and expenses whatsoever (including, without limitation, incidental, special and consequential damages) resulting from any use of or reliance on the information contained herein, whether based on warranty, contract, tort or any other legal theory, and whether or not Newport has been advised of the possibility of such damages.

Newport does not guarantee the availability of any products or software and reserves the right to discontinue or modify its products and software at any time. Users of the products or software described herein should refer to the User's Manual and other documentation accompanying such products or software at the time of sale or license for more detailed information regarding the handling, operation and use of such products or software, including but not limited to important safety precautions.

This Application Note shall not be copied, reproduced, distributed or published, in whole or in part, without the prior written consent of Newport Corporation.

ISO 9001
FM 27207

Newport Corporation, Irvine, California, has been certified compliant with ISO 9001 by the British Standards Institution.

MM#9000101
DS-04091